Journal of Nuclear Materials 448 (2014) 26–32

Contents lists available at ScienceDirect

Journal of Nuclear Materials

journal homepage: www.elsevier.com/locate/jnucmat

Sensitivity of ultrasonic nonlinearity to irradiated, annealed, and re-irradiated microstructure changes in RPV steels

K.H. Matlack [a,*], J.-Y. Kim [b], J.J. Wall [a,c], J. Qu [d], L.J. Jacobs [a,b], M.A. Sokolov [e]

[a] G.W. Woodruff School of Mechanical Engineering, Georgia Institute of Technology, Atlanta, GA 30332, United States
[b] School of Civil and Environmental Engineering, Georgia Institute of Technology, Atlanta, GA 30332, United States
[c] Electric Power Research Institute, Charlotte, NC 28262, United States
[d] Department of Civil and Environmental Engineering, Northwestern University, Evanston, IL 60208, United States
[e] Metals and Ceramics Division, Oak Ridge National Laboratory, Oak Ridge, TN 37831, United States

ARTICLE INFO

Article history:
Received 23 October 2013
Accepted 22 January 2014
Available online 28 January 2014

ABSTRACT

The planned life extension of nuclear reactors throughout the US and abroad will cause reactor vessel and internals materials to be exposed to more neutron irradiation than was originally intended. A nondestructive evaluation (NDE) method to monitor radiation damage would enable safe and cost-effective continued operation of nuclear reactors. Radiation damage in reactor pressure vessel (RPV) steels causes microstructural changes that leave the material in an embrittled state. Nonlinear ultrasound is an NDE technique quantified by the measurable acoustic nonlinearity parameter, which is sensitive to microstructural changes in metallic materials such as dislocations, precipitates and their combinations. Recent research has demonstrated the sensitivity of the acoustic nonlinearity parameter to increasing neutron fluence in representative RPV steels. The current work considers nonlinear ultrasonic experiments conducted on similar RPV steel samples that had a combination of irradiation, annealing, re-irradiation, and/or re-annealing to a total neutron fluence of 0.5–5 $\times$ 10^{19} n/cm^2 (E > 1 MeV) at an irradiation temperature of 290 °C. The acoustic nonlinearity parameter generally increased with increasing neutron fluence, and consistently decreased from the irradiated to the annealed state over different levels of neutron fluence. Results of the measured acoustic nonlinearity parameter are compared with those from previous measurements on other RPV steel samples. This comprehensive set of results illustrates the dependence of the measured acoustic nonlinearity parameter on neutron fluence, material composition, irradiation temperature and annealing.

1. Introduction

Radiation damage in nuclear reactor pressure vessels (RPV) is a growing concern as nuclear plants seek license renewal beyond the intended 40 years of operation to 60 years and possibly further. Exposure of RPV steels to neutron radiation causes point defects that have been shown to ultimately evolve into microstructural features such as vacancy-solute complexes, solute clusters, dislocation loops, and copper-rich precipitates [1–4]. These microstructural features leave the material in an embrittled state, causing a shift in the ductile-brittle transition temperature (DBTT), an increase in yield stress, and leaving the material more susceptible to irradiation assisted stress corrosion cracking [1,5]. In steels containing copper over about 0.05–0.1% Cu, copper-rich precipitates have been shown to be the primary contributor to radiation embrittlement [1]. The evolution of microstructural features and thus the progression of radiation embrittlement is highly dependent on multiple variables: neutron fluence, neutron flux, irradiation temperature, material composition, initial microstructure, and the energy spectrum of the neutrons [2,6–9]. It is of upmost importance to ensure that increased radiation damage to the RPV does not cause, for example, such a drastic shift in the DBTT that the reactor is operating in the brittle fracture regime. One potential method of mitigating radiation-induced embrittlement in the RPV is thermal annealing of the RPV [10], which has been shown to effectively recover some or most of the radiation embrittlement, depending on the material, irradiation, and annealing parameters [2,11,12]. However, microstructural changes after such post-irradiation annealing (PIA) treatments, following re-irradiation, and the resulting embrittlement in these cases are still areas of ongoing research [13,14].

Current methods of radiation damage monitoring include extensive macro-, micro-, and nano-structural analysis on surveillance samples, which were placed in the reactor at the start of operation and periodically removed for testing to correlate to the

* Corresponding author. Tel.: +1 404 894 2344.
E-mail address: katie.matlack@gatech.edu (K.H. Matlack).

http://dx.doi.org/10.1016/j.jnucmat.2014.01.038
0022-3115/

actual radiation-induced damage of the RPV structure. In addition, there are widespread efforts on modeling and characterization of material irradiated in test reactors operated at higher flux to achieve relevant levels of neutron fluence over a shorter period of time. A nondestructive evaluation method to characterize radiation damage in the RPV could be a powerful complementary tool in quantifying the remaining strength of these structures.

The nonlinear ultrasonic technique of second harmonic generation is a nondestructive evaluation method that is sensitive to microstructural changes in metallic materials. As an incident sinusoidal wave propagates through a nonlinear elastic medium, a second harmonic wave is generated from its interaction with microstructural features such as dislocations, dislocations dipoles, and precipitates; this second harmonic wave is quantified by the acoustic nonlinearity parameter, β [15–19]. Previous research has shown that nonlinear ultrasound is sensitive to damage mechanisms such as fatigue [16,20–22], cold work [23], thermal aging [19,24–26], and creep [27]. Nonlinear ultrasound has recently been shown to be sensitive to radiation damage in RPV steels [28] by measuring changes in the acoustic nonlinearity parameter, β, due to increases in neutron fluence of two representative RPV steels.

This paper investigates the effect of various parameters – neutron fluence, irradiation temperature, copper content, PIA and re-irradiation – and thus the resulting radiation-induced microstructural changes in RPV steel, on the measured acoustic nonlinearity parameter. This work provides further evidence of the applicability of nonlinear ultrasound as a nondestructive evaluation tool to characterize radiation damage in RPV steels.

2. Nonlinear ultrasound

2.1. Theoretical considerations

Consider a sinusoidal longitudinal wave propagating at frequency ω through a weakly nonlinear elastic material. A second harmonic wave at frequency 2ω is generated through the interaction of the propagating wave with the nonlinear medium. The acoustic nonlinearity parameter, β, that quantifies this second harmonic wave has been shown to have the following relation [15]:

$$\beta = \frac{8A_2}{A_1^2\kappa^2 x}, \tag{1}$$

where A_2 is the amplitude of the second harmonic wave generated, A_1 is the amplitude of the propagated first harmonic wave, κ is the wave number, and x is the wave propagation distance.

It has previously been shown both theoretically and experimentally how different microstructural features that are relevant to radiation damage in RPV materials give rise to changes in β. The change in β due to a density of dislocations, Λ, that are pinned between two points to create a dislocation segment length of L_0, with some internal stress, σ_0, has been shown to be [15].

$$\Delta\beta \propto \Lambda L_0^4\sigma_0. \tag{2}$$

This initial internal stress σ_0 is expected to be small, and note that the pinning points that create the dislocation segment length are features such as grain boundaries, other dislocations, and/or point defects.

Now assume that there is some distribution of precipitates embedded in the microstructure, which act as discrete pinning points for dislocations. We assume some number density of precipitates, N, with average radius r_p. For this case, the change in β has been shown to be [19,24]:

$$\Delta\beta \propto \frac{\Lambda r_p^3}{N^{1/3}}. \tag{3}$$

Here, the stress in the material is due to a misfit strain of the precipitate embedded in the matrix, which is expected to be much larger than the initial stress σ_0. The full expression for the radial stress due to a spherical precipitate embedded in the microstructure can be found elsewhere [19,24,29,30]. The relationship between segment length and number density of precipitates is assumed to be $L \approx 1/N^{1/3}$ as in previous work [24].

However, there should be some critical number density of precipitates, N_{cr}, only above which this precipitate-pinned dislocation contribution to β applies. The critical density corresponds to the density when all dislocations are pinned at least once in their lengths and therefore it is a constant multiple of the initial dislocation density. Above this critical density, additional precipitates will only shorten the lengths of the already-pinned dislocation segments. Therefore, the evolution of β is likely to follow some combination of the general dislocation pinning model (Eq. (2)) and the precipitate-pinned dislocation model (Eq. (3)), which can be expressed as:

$$\Delta\beta \propto (1-\alpha)\Lambda L_0^4\sigma_0 + \alpha\Lambda\frac{r_p^3}{N^{1/3}}, \tag{4}$$

where α represents the probability of forming the 3-precipitate cluster to bend an existing dislocation segment. This probability is close to zero at very low precipitate density, and is assumed to increase rapidly to 1 at N_{cr}. It is expected that α increases exponentially to 1 because the probability of an additional precipitate to interact with a dislocation depends on the precipitate concentration at the moment when the additional precipitate is added. Further, once the precipitate number density reaches N_{cr}, the chance for any additional nucleated precipitate to interact with a dislocation is nearly 100%. In this way, it is assumed the probability follows Boltzmann statistics, which represents the chance of a group of precipitates to form a specific configuration near a dislocation line, such that $\alpha = \exp(-B/N)$, where B is a positive number representing the precipitate configurational entropy and N is the current precipitate density.

The parameter α is also equivalent to the volume fraction of precipitate-pinned dislocation segments, such that the term $(1-\alpha)$ represents the volume fraction of dislocations pinned by other features (e.g. grain boundaries, other dislocations, impurities, point defects, vacancies, or voids). Note that both the model of generally pinned dislocations (Eq. (2)) and the model of precipitate-pinned dislocations (Eq. (3)) cannot apply at the same time to the same dislocation segment – if a dislocation segment is pinned by two precipitates, that same segment cannot also be pinned by other features. It is expected that the first term in Eq. (4) would dominate the behavior of β in the initial stages of radiation damage when precipitates are beginning to form. Then, as the number density of precipitates increases close to the N_{cr}, the second term in Eq. (4) would dominate the trend of β.

2.2. Experimental method

Contact piezoelectric ultrasonic transducers, with diameter 6.35 mm, were mounted on either side of a 10 mm-thick sample with a light oil coupling. The transducer material was lithium niobate, and center frequencies of the transducers were chosen to approximate the first and second harmonic frequencies. The sample and transducers were mounted and aligned in a specially designed fixture for accurate alignment and consistent clamping [31]. A schematic of the measurement setup is shown in Fig. 1. A function generator (Agilent 33250A) generated a 12-cycle sinusoidal wave at 3.3 MHz, amplified with a high-power gated amplifier (RITEC GA2500A), in the 3.5 MHz center frequency of the transmitting transducer. The ultrasonic signal propagated through the

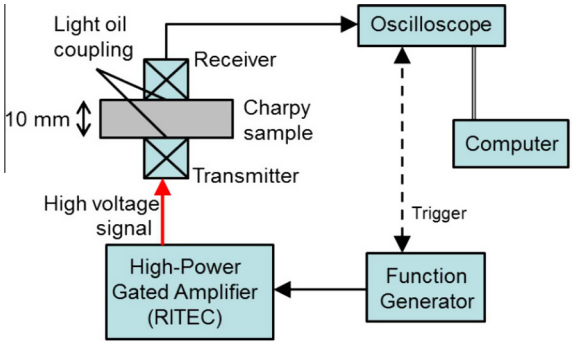

Fig. 1. Schematic of experimental setup for nonlinear ultrasonic measurements.

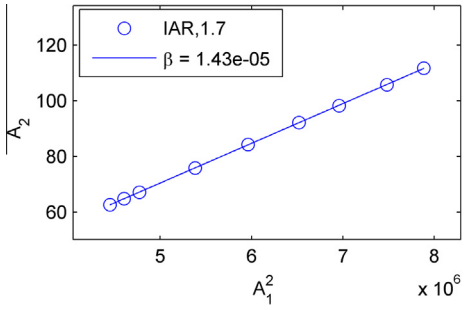

Fig. 3. Representative data for measurement of β in IAR,1.7, by calculating slope of linear fit between A_2 and A_1^2.

thickness of the sample and the receiving transducer, with center frequency of 7.5 MHz, simultaneously detected the first and second harmonic waves. The signal was then transferred to an oscilloscope (Tektronix TDS 5034B) and then to a computer for post-processing. The steady-state portion of the time signal was extracted, a Hann window applied, and the fast-Fourier transform computed; a representative time signal and frequency response is shown in Fig. 2. The first and second harmonic amplitudes were extracted from the frequency response, and the process repeated for a total of nine measurements of increasing input voltage. The slope of the linear fit of the data A_2 and ${A_1}^2$ is a relative measure of β, as illustrated in Fig. 3, i.e. $\beta \propto A_2/A_1^2$. Results are presented in terms of a change in β, relative to the unirradiated state. Note that while this procedure does not produce an absolute measurement of β, effects of nonlinearities from instrumentation are still eliminated since all measurements are compared to a baseline measurement. Absolute measurements were not feasible due to time limitations in handling the radioactive samples.

3. Materials investigated

The samples measured in this study were IAEA reference material JRQ (A533 grade B class 1) with the chemical composition given in Table 1. These samples were irradiated in the 10 MW (thermal) SAPHIR reactor at Paul Scherrer Institute (PSI), at an irradiation temperature of T_{ir} = 290 °C and at a neutron flux of roughly 5×10^{12} n/cm^2 s. These samples were part of a previous study with PSI and Oak Ridge National Laboratory (ORNL) [12,13]. Samples were irradiated to a total neutron fluence of 0.5–5.0 $\times$ 10^{19} n/cm^2, and some samples were given an annealing treatment of 460 °C/18 h when 50% of the target fluence was reached. Two other samples were then given a second annealing treatment of 460 °C/18 h after the full neutron fluence was reached. A total of five sample conditions were investigated, and the conditions are given in detail in Table 2. Note that in this table and throughout this work, the sample designations use the following abbreviations:

Table 1
Chemical composition (wt.%) of JRQ and JFL materials.

Material	C	Si	Mn	Cr	Mo	Ni	P	Cu	S
JRQ	0.18	0.24	1.42	0.12	0.51	0.84	0.017	0.14	0.004
JFL	0.17	0.25	1.42	0.16	0.52	0.75	0.004	0.01	0.002

unirradiated (U), irradiated (I), annealed (A), and re-irradiated (R). The sample geometry was a broken half of a standard Charpy-V sample, with dimensions of 10 mm $\times$ 10 mm $\times$ 27 mm, with wave propagation through one of the 10 mm dimensions, which was kept consistent among all samples and measurements. Sample surfaces were hand polished with up to 600 grit polish paper and cleaned in an ultrasonic bath, to sufficiently prepare surfaces for the nonlinear ultrasonic measurements.

This sample set enabled an investigation of effects from post-irradiation annealing and re-irradiation, and also enabled an analysis of the influence of irradiation temperature on the measured β. Results of measurements on these samples are compared in the current work to measurements of β on other irradiated RPV material, where measurements of β were made on samples irradiated at a temperature of 255 °C [28]. This previous sample set [28] contained two different RPV materials: the same JRQ as in the current study (though with slightly different mechanical properties, see [12,32]) and a low-copper material referred to as JFL (forged ASTM A508 Cl.3). The main differences between these two materials are their Cu and P content – JRQ contains a higher concentration of Cu (0.14 wt.%) and P (0.017 wt.%) than JFL (Cu: 0.01 wt.%, P: 0.004). The chemical composition of these materials is also given in Table 1, and details of the irradiations are provided in Table 2. Further details of that investigation are given elsewhere [28].

4. Results

Results for the measured β as a function of increasing fluence and the influence of post-irradiation annealing and re-irradiation

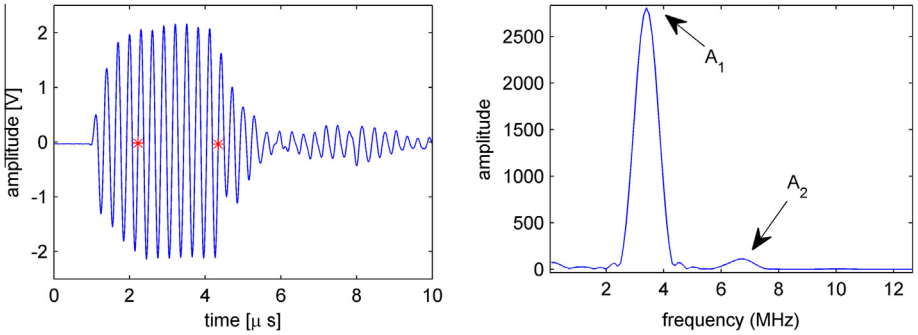

Fig. 2. Representative time signal (left) and FFT (right) of measurement on IAR,1.7 sample. The starred points indicated on the time signal show the points between which the FFT was calculated.

Table 2
Conditions for samples undergoing irradiation, post-irradiation annealing, re-irradiation, and re-annealing. Neutron fluence and flux levels are all in terms of neutron energies of $E > 1$ MeV.

Material	Irradiation temp.	Designation	Irradiation (10^{19} n/cm^2)	Anneal	Re-irradiation (10^{19} n/cm^2)/ re-anneal	Flux (10^{12} n/cm^2)
JRQ (heat 1)	290 °C	U	–	–	–	–
		UA	–	460 °C/18 h	–	–
		IAR,0.5	0.25	460 °C/18 h	0.25	5.0
		IARA,0.5	0.25	460 °C/18 h	0.25, annealed 460 °C/18 h	5.0
		IAR,1.7	0.85	460 °C/18 h	0.25	5.0
		IARA,1.7	0.85	460 °C/18 h	0.85, annealed 460 °C/18 h	5.0
		I,5	5.0	–	–	5.0
		IA,5	5.0	460 °C/18 h	–	5.0
JRQ (heat 2)	255 °C	U	–	–	–	–
		I,5.4	5.4	–	–	3.01
		I,9.8	9.8	–	–	5.37
JFL	255 °C	U	–	–	–	–
		I,5.1	5.1	–	–	2.82
		I,8.6	8.6	–	–	4.74

of JRQ material irradiated at 290 °C are given in Fig. 4. Each data point represents an average over three separate measurements on the same sample at the same location, and error bars indicate one standard deviation from the mean. Separate data points for the same sample condition represent measurements on separate Charpy halves of the same sample condition, or measurements at different locations along the length of the Charpy half. The results in Fig. 4 show little variation among locations and between different sample halves when compared to the changes due to irradiation and annealing; these spatial and sample variations in the same Charpy sample are shown to be insignificant. The measured β increased from the unirradiated state to the maximum neutron fluence, with a maximum increase of 18% at 5×10^{19} n/cm^2 ($E > 1$ MeV). Results show a decrease in measured β from the irradiated condition (I or IAR) to the annealed condition (IA or IARA) – a 23.2% decrease due to annealing in the I,5 and IA,5 samples, and a 25.7% decrease due to annealing in the IAR,1.7 and IARA,1.7 samples. A summary of these changes in β due to neutron fluence and then due to annealing is given in Table 3. Note that the intermediate anneal in samples IAR,0.5 and IAR,1.7 effectively recovered most of the irradiation-induced embrittlement during the first irradiation to half the target fluence [12], so a more representative value for the neutron fluence of these samples in terms of β might be half the fluence listed in Table 3.

Previous results for measured β for JRQ and JFL material at $T_{ir} = 255$ °C as a function of increasing neutron fluence are shown together with the current results of measured β for irradiated JRQ at $T_{ir} = 290$ °C in Fig. 5. Results for JRQ at $T_{ir} = 290$ °C in Fig. 5 have been averaged over all measurements on different Charpy halves and different locations. Note that light water reactor pressure vessels typically operate at 290 °C ± 30°, so the irradiation temperatures of the two data sets considered in this study approximate vessel operational conditions [1]. These results are presented in terms of a normalized β to the unirradiated state in each sample set, i.e. $\beta_i/\beta_0 = (A_2/A_1^2)_i/(A_2/A_1^2)_0$. In this way, the dependence of β on the input fundamental radial frequency, ω, is eliminated, such that different excitation frequencies used in the measurements ($f = 2.25$ MHz for $T_{ir} = 255$ °C and $f = 3.3$ MHz for $T_{ir} = 290$ °C, where $\omega = 2\pi f$) do not influence the relative comparison of the measured β. Note that differences in fundamental frequency were due to limitations in equipment during earlier experiments – higher frequencies are more ideal for the shorter wave propagation distances encountered in these experiments, since the shorter wavelength allows more cycles and thus higher amplitude of A_2, given the same sample thickness.

The trend of β as a function of neutron fluence for the irradiated JRQ at $T_{ir} = 290$ °C is similar to the trend shown in the previous work [28] and as seen in Fig. 5 – an increase in β up to a medium fluence of roughly 5×10^{19} n/cm^2. However, the increase in β is

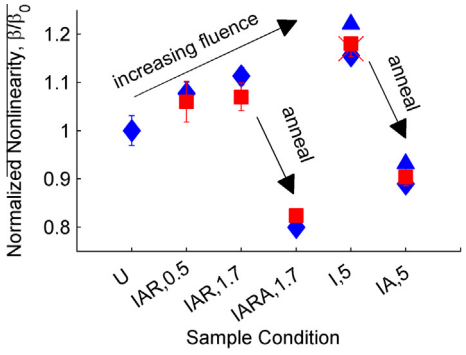

Fig. 4. Results of measured β for irradiated, annealed, re-irradiated, and re-annealed samples, over increasing neutron fluence and showing effects of annealing. Data points represent measurements on the first Charpy half at location 1 (♦) and location 2 (▲), and on the second Charpy half at location 1 (■) and location 2 (X).

Table 3
Change in β due to annealing and increased neutron fluence of JRQ ($T_{ir} = 290$ °C).

Total neutron fluence	$\Delta\beta$ from annealing	$\Delta\beta$ from irradiation (%)
0.5×10^{19} n/cm^2	–	+7
1.7×10^{19} n/cm^2	−25.7%	+9
5×10^{19} n/cm^2	−23.2%	+18

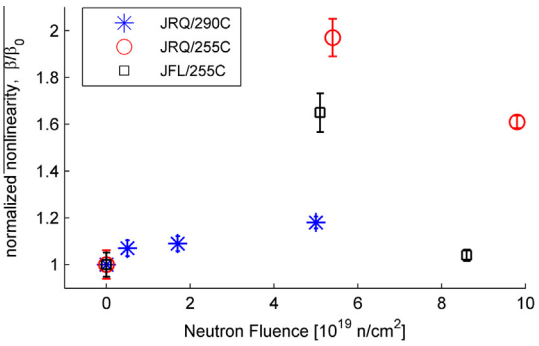

Fig. 5. Influence of increasing neutron fluence ($E > 1$ MeV) on β, for JRQ and JFL at $T_{ir} = 255$ °C and 290 °C. Each dataset is normalized to the measured β in the unirradiated state, β_0. JRQ samples irradiated at 290 °C to 0.5×10^{19} and 1.7×10^{19} n/cm^2 received an intermediate anneal at 50% target fluence.

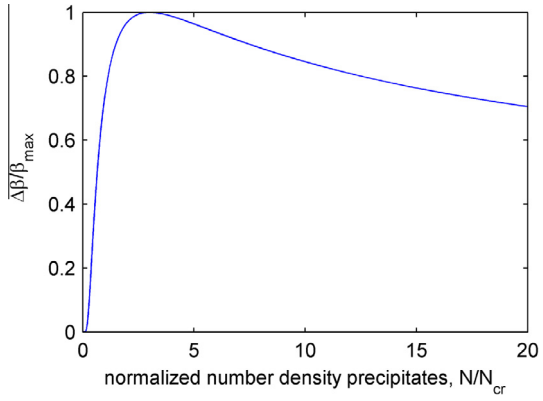

Fig. 6. Predicted trend of $\Delta\beta$ (normalized by β_{max}) as a function of number density of precipitates, normalized by N_{cr}, assuming trend is dominated by precipitate-pinned dislocations (i.e. second term in Eq. (4)).

much more pronounced in the samples with T_{ir} = 255 °C, even in the low-copper alloy of JFL. At a neutron fluence of 5×10^{19} n/cm^2, it is shown that at T_{ir} = 255 °C, β increased by almost 100% in JRQ and 65% in JFL, while at T_{ir} = 290 °C, β increased by only 18% in JRQ, all from the respective unirradiated conditions of each sample set. These results show that the acoustic nonlinearity parameter strongly depends on the irradiation temperature as well as the level of neutron fluence.

5. Discussion

In low-alloy steels under typical RPV conditions, neutron irradiation causes radiation-enhanced diffusion, which results in microstructural features such as copper-rich precipitates, solute clusters, matrix defects in the form of solute-vacancy complexes, and potentially dislocations and interstitial loops [1–3]. Considering the model described in Eq. (4) for the change in β due to pinned dislocations, and assuming the precipitate-pinned contribution is stronger due to the higher stress induced by the precipitate misfit, β should *generally* increase by $\exp(-B/N)/N^{1/3}$ below N_{cr}, and decrease by $N^{1/3}$ above N_{cr}. The plot in Fig. 6 illustrates this trend, and note that for simplicity we assume $B = 1$ such that the plot shows the function $\Delta\beta = \exp(-1/N)/N^{1/3}$. Since the change in $\Delta\beta$ over neutron fluence for T_{ir} = 255 °C changes sign at the medium fluence of roughly 5×10^{19} n/cm^2, we can infer that N_{cr} occurs roughly around this fluence level. Comparison of this model with experimental results suggest that in the JRQ samples irradiated at 290 °C, the number density of precipitates is below N_{cr}, which explains the increasing measured β with increasing neutron fluence, and likely increasing number density of precipitates. This model qualitatively agrees with the experimental results, but suggests there are other microstructural features that contribute to the total $\Delta\beta$.

Previously, small angle neutron scattering (SANS) experiments were conducted on the same JRQ and JFL samples with T_{ir} = 255 °C reported on here and previously [28], to quantify these microstructural features. The authors reported an increase in volume fraction of precipitates with constant average radius of about 1 nm with increasing neutron fluence [33]. Specifically, the volume fraction increased from 0.005–0.09 vol.% for neutron fluence of 0.7–8.7 $\times 10^{19}$ n/cm^2 in JFL, and 0.21–0.5 vol.% for neutron fluence of 0.7–9.8 $\times 10^{19}$ n/cm^2 for JRQ. Considering the precipitate-pinned dislocation theory, this would imply that $\Delta\beta$ should be lower in JRQ compared to JFL, since JRQ has a higher volume fraction of copper rich precipitates. However, experimental evidence in Fig. 5 shows the opposite – $\Delta\beta$ is larger for JRQ. Differences between the two materials such as dislocation density, grain structure (which would influence general dislocation pinning effects by grain boundaries), point defects and other defects, and different N_{cr} could all contribute to this discrepancy. This again suggests that there are other microstructural features that contribute to the total $\Delta\beta$, and more microstructural characterizations are needed to explain this.

Microstructural changes over increasing neutron fluence are dependent on many other factors such as neutron flux, irradiation temperature, and material composition. For example, a rapid increase, followed by saturation, followed by slow coarsening and a decrease in number density of precipitates was predicted by models and confirmed experimentally for 0.3% Cu RPV steels irradiated at low neutron flux and 290 °C [2]. As another example, it has been shown that an increase in the nickel content in irradiated RPV material correlates to an increase in both average radius and number density of copper-rich precipitates [8]. Further, changes in the irradiation temperature particularly in the range of about 250-300 °C, as well as the neutron flux has been shown to strongly affect how the microstructure evolves over increasing neutron fluence [2,9,34]. The following sections provide a discussion on other possible contributions of microstructural features to β, in terms of reported microstructural evolutions over the relevant irradiation conditions in the current study.

5.1. Effects of neutron flux and composition

The effect of higher fluxes typical of test reactors depends on the combination of copper content, irradiation temperature, and neutron fluence [2,35]. It has been shown that in low Cu steels, higher flux typical of test reactors can produce increased hardening at higher fluence due to an increased amount of unstable matrix defects (UMDs) [2,36]. In contrast, in higher Cu steels, these UMDs act as sinks to delay precipitation from radiation-enhanced diffusion [2], and thus delay or reduce hardening. This flux-dependent regime has been estimated to begin at fluxes above about 5×10^{11} n/(cm^2 s) at T_{ir} = 290 °C [34]. So, it is likely that these flux-related effects occur and cause different effects in the trend of $\Delta\beta$ in the lower temperature samples of irradiated JRQ and JFL at T_{ir} = 255 °C.

Recall that the JFL samples contained 0.01% Cu (low-copper steel), and the JRQ samples contained 0.14% Cu (medium-copper steel). It has been shown that the dominating hardening mechanisms in low-copper steels are other defects and matrix features such as point defect clusters and manganese-nickel precipitates [2,8,35]. It is plausible that these defects, as well as UMDs as suggested in [2,36], have formed in the high fluence samples of the low-Cu JFL material, creating more pinning points for dislocations and thus causing a decrease in β, which would align with the experimental results.

5.2. Effects of Irradiation temperature

Irradiation hardening due to matrix features (namely vacancy-solute cluster complexes) has been shown to increase with decreasing irradiation temperature, since matrix features are more thermally stable at lower temperatures [2,9]. A lower irradiation temperature has also been shown to increase both the volume fraction and number density of precipitates, while decreasing the radius of the precipitates in the range of T_{ir} = 270–310 °C [8]. This indicates that it is expected that there should be a smaller number density of precipitates in the JRQ at 290 °C compared to JRQ at 255 °C at the common neutron fluence of 5×10^{19} n/cm^2. Therefore, it can be assumed that the critical number density of precipitates, N_{cr}, has not yet been reached in the JRQ T_{ir} = 290 °C samples and thus β is expected to increase generally with increasing N,

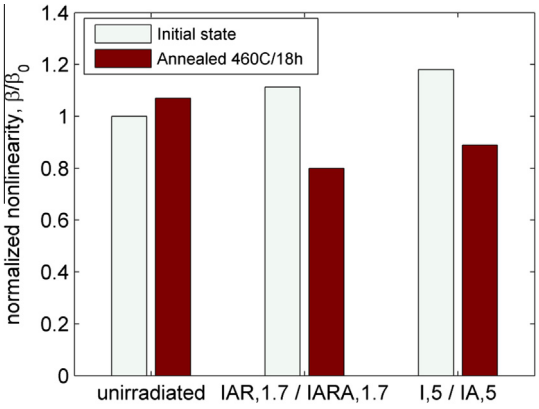

Fig. 7. Dependence of β on annealing microstructural for unirradiated JRQ and irradiated JRQ (T_{ir} = 290 °C).

since $N < N_{cr}$ in this case. This can potentially explain the differences in $\Delta\beta$ in JRQ at roughly 5×10^{19} n/cm^2 for T_{ir} = 290 °C ($\Delta\beta$ = +18%) and T_{ir} = 255 °C ($\Delta\beta$ = +97%). Small angle neutron scattering (SANS) measurements could confirm this.

5.3. Post-irradiation annealing

Post-irradiation annealing (PIA) has been shown to recover some of the irradiation-induced embrittlement in RPV steels [2,11–13]. Nanstad et al. [12] conducted Charpy impact testing on the JRQ samples investigated in the current work, and showed almost full recovery of the irradiation-induced ductile-brittle transition temperature shift from the annealing treatment. In a follow-up study, atom probe tomography (APT) experiments showed a decrease in number density of copper-rich precipitates of about an order of magnitude [13]. The remaining precipitates in the microstructure were significantly larger, and were only observed near grain boundaries. Follow-up characterizations are needed to fully quantify the changes in number density and size of precipitates in the PIA state, but the APT results showed that annealing caused most of the copper to dissolve in the matrix, while the remaining copper precipitates grew and coarsened. This effect of PIA has been shown in other studies, for example with VVER-440 weld material interrogated with APT and positron annihilation spectroscopy (PAS) [14,37], and with SANS measurements of high-copper RPV weld materials [37].

To isolate contributions to β from annealing effects on the irradiated microstructure, an unirradiated JRQ sample was annealed with the same schedule as the post-irradiation annealing (460 °C/18 h). A slight increase in β of 7% was measured in the unirradiated and annealed sample, compared to the purely unirradiated sample. These results are shown in Fig. 7, in comparison with the change in β due to annealing in the irradiated samples, where a clear decrease of 23–26% was seen from irradiated to annealed state. Since no (or at least very few) precipitates are expected to be present in the unirradiated sample, the results clearly show that the change in β from PIA is due to changes specific to the irradiated microstructure.

The number density of precipitates in I,5 and IAR,1.7 samples should be below N_{cr} as defined in Section 2. Therefore, as precipitates are removed from the microstructure, N should still be below N_{cr}, and as such β should generally decrease as indicated by Eq. (4) and Fig. 6. Experimental evidence clearly shows this decrease in β. It is also possible that the coarsened precipitates remaining in the annealed microstructure have become incoherent with the matrix. The stress surrounding incoherent precipitates is significantly less than coherent precipitates, such that the precipitate-pinned dislocation model no longer applies.

5.4. Re-irradiation effects

It has been shown that microstructural evolution during re-irradiation following PIA follows a different path than a purely irradiated microstructure [13,14]. Nanstad et al. [13] conducted atom probe tomography investigations on the current samples, and they reported that re-irradiation does cause copper-rich precipitates to form with a number density similar to that in the irradiated only condition, but with a smaller radius. If only considering the precipitate-pinned dislocation contribution to the nonlinearity parameter, the measured β should scale by $(r_{IAR}/r_I)^3$ when comparing a purely irradiated sample to an irradiated-annealed-re-irradiated sample to the same total fluence. Here, r_{IAR} is the radius of precipitates in the IAR condition, and r_I is the radius of precipitates in the irradiated condition.

Note that the samples at the lower neutron fluence levels for JRQ at T_{ir} = 290 °C were given an annealing treatment when 50% of the target fluence was reached. This annealing was shown to recover a significant portion of the change in ductile-brittle transition temperature due to irradiation [12,13]. So it is possible that a more representative measure of neutron fluence in terms of microstructural features is only the amount of neutron fluence received during the re-irradiation. In other words, 0.25×10^{19} n/cm^2 (instead of 0.5×10^{19} n/cm^2) might be a more representative fluence for sample IAR,0.5, and 0.85×10^{19} n/cm^2 (instead of 1.7×10^{19} n/cm^2) might be a more representative fluence for sample IAR,1.7. However, re-irradiation following post-irradiation annealing has been shown in some cases to follow a different path for microstructural evolution compared to changes due to the initial irradiation [14]. For example, Kuramoto et al. [14] investigated re-irradiation effects in VVER-440 type weld material, and concluded from APT and PAS studies that matrix defects are the primary hardening mechanism in the re-irradiated state. So, it is possible that matrix defects contribute to the measured β in IAR samples measured in the current study. It has been shown that defects such as vacancies can act in the same way as precipitates in terms of pinning points to dislocations [18]. It is also possible that these matrix defects respond as a different mechanism for contributing to the nonlinearity parameter. Further studies are needed to fully realize the effects on β from microstructural evolution during re-irradiation.

6. Conclusions

Nonlinear ultrasonic measurements of the acoustic nonlinearity parameter, β, were made on a set of Charpy-V samples of JRQ (ASTM A533 grade B class 1), a representative reactor pressure vessel steel material. The samples were previously irradiated, and some were further treated with post-irradiation annealing, re-irradiation, and/or re-annealing, to a total neutron fluence of 0.5–5×10^{19} n/cm^2 (E > 1 MeV) at T_{ir} = 290 °C. These nonlinear ultrasonic measurements show that the experimentally measured β increases with increasing levels of neutron fluence. In addition, these measurements show a consistent decrease in the measured β due to annealing from either the irradiated or re-irradiated state. Comparison with previous results [31] on JRQ and JFL samples at T_{ir} = 255 °C shows a qualitatively similar trend for the measured β with increasing neutron fluence up to 5×10^{19} n/cm^2 (E > 1 MeV), but with a strong dependence on irradiation temperature. A theoretical model of the contribution of precipitate-pinned dislocations to changes in β is consistent with experimental measurements. These results show that the measured acoustic

nonlinearity parameter strongly depends on the irradiation temperature as well as the level of neutron fluence, and can detect microstructure changes due to post-irradiation annealing. Nonlinear ultrasound can therefore detect microstructural changes due to different irradiation conditions, and shows potential as a viable nondestructive evaluation method for monitoring radiation damage in RPV steel.

Acknowledgements

The authors thank the staff at Oak Ridge National Laboratory for assistance in preparing and handling the irradiated materials. This research is being performed using funding received from the DOE Office of Nuclear Energy's Nuclear Energy University Programs. Additional funding has been provided by the Electric Power Research Institute (EPRI). This work was also supported by the National Science Foundation through a Graduate Research Fellowship to Kathryn Matlack.

References

[1] G.R. Odette, G.E. Lucas, JOM 53 (2001) 18–22.
[2] G.R. Odette, G.E. Lucas, Radiat Effects Defects Solids: Incorp Plasma Sci Plasma Technol 144 (1998) 189–231.
[3] E. Meslin, M. Lambrecht, M. Hernandez-Mayoral, F. Bergner, L. Malerba, P. Pareige, B. Radiguet, A. Barbu, D. Gomez-Briceno, A. Ulbricht, A. Almazouzi, J. Nucl. Mater. 406 (2010) 73–83.
[4] N. Soneda, K. Dohi, K. Nishida, A. Nomoto, M. Tomimatsu, H. Matsuzawa, J. ASTM Int. 6 (2009).
[5] G.S. Was, Fund. Radiat. Mater. Sci., Springer, 2007.
[6] J.T. Buswell, W.J. Phythian, R.J. McElroy, S. Dumbill, P.H.N. Ray, J. Mace, R.N. Sinclair, J. Nucl. Mater. 225 (1995) 196–214.
[7] G.R. Odette, G.E. Lucas, D. Klingensmith, in: R.G. Elliman, M.A.K. Jr., G.E. Lucas, L.L. Snead (Eds.), Materials Research Society Symposium, vol. 650, Materials Research Society, 2001, pp. R6.4.1–R6.4.6.
[8] E.D. Eason, G.R. Odette, R.K. Nanstad, T. Yamamoto, ORNL/TM-2006/530, 2006.
[9] E.D. Eason, G.R. Odette, R.K. Nanstad, T. Yamamoto, J. Nucl. Mater. 433 (2013) 240–254.
[10] Title 10, Code of Federal Regulations, Parts 0 to 199, U.S. Government Printing Office, 1987.
[11] E.D. Eason, J.E. Wright, E.E. Nelson, G.R. Odette, E.V. Mader, Nucl. Eng. Des. 179 (1998) 257–265.
[12] R.K. Nanstad, P. Tipping, R.D. Kalkhof, M.A. Sokolov, in: M.L. Grossbeck, T.R. Allen, R.G. Lott, A.S. Kumar (Eds.), The Effects of Radiation on Materials: 21st International Symposium, ASTM STP 1447, ASTM International, West Conshokocken, PA, 2004, pp. 149–163.
[13] R.K. Nanstad, M. Niffenegger, R.D. Kalkhof, M.K. Miller, M.A. Sokolov, P. Tipping, J. ASTM Int. 2 (2005) 1–17.
[14] A. Kuramoto, T. Toyama, Y. Nagai, K. Inoue, Y. Nozawa, M. Hasegawa, M. Valo, Acta Mater. 61 (2013) 5236–5246.
[15] A. Hikata, B.B. Chick, C. Elbaum, J. Appl. Phys. 36 (1965) 229–236.
[16] J.H. Cantrell, W.T. Yost, Int. J. Fatigue 23 (2001) S487–S490.
[17] M.A. Breazeale, D.O. Thompson, Appl. Phys. Lett. 3 (1963) 77–78.
[18] J.H. Cantrell, Philos. Mag. 86 (2006) 1539–1554.
[19] J.H. Cantrell, X.G. Zhang, J. Appl. Phys. 84 (1998) 5469–5472.
[20] J. Frouin, S. Sathish, T.E. Matikas, J.K. Na, J. Mater. Res. 14 (1998) 1295–1298.
[21] J.-Y. Kim, L.J. Jacobs, J. Qu, J.W. Littles, J. Acoust. Soc. Am. 120 (2006) 1266–1273.
[22] S.V. Walker, J.-Y. Kim, J. Qu, L.J. Jacobs, NDT&E Int. 48 (2012) 10–15.
[23] A. Viswanath, B.P.C. Rao, S. Mahadevan, P. Parameswaran, T. Jayakumar, B. Raj, J. Mater. Process. Technol. 211 (2011) 538–544.
[24] D.C. Hurley, D. Balzar, P.T. Purtscher, J. Mater. Res. 15 (2000) 2036–2042.
[25] D.J. Barnard, G.E. Dace, O. Buck, J. Nondestr. Eval. 16 (1997) 67–75.
[26] A. Ruiz, N. Ortiz, A. Medina, J.-Y. Kim, L.J. Jacobs, NDT&E Int. 54 (2013) 19–26.
[27] S. Baby, B.N. Kowmudi, C.M. Omprakash, D.V.V. Satyanarayana, K. Balasubramaniam, V. Kumar, Scr. Mater. 59 (2008) 818–821.
[28] K.H. Matlack, J.J. Wall, J.-Y. Kim, J. Qu, L.J. Jacobs, H.-W. Viehrig, J. Appl. Phys. 111 (2012) 054911–054913.
[29] J.W. Martin, in: Precipitation Hardening, Pergamon Press, Great Britian, 1968, pp. 60–63.
[30] J.H. Cantrell, W.T. Yost, Appl. Phys. Lett. 77 (2000) 1952–1954.
[31] K.H. Matlack, J. Wall, J.-Y. Kim, L.J. Jacobs, J. Qu, H.-W. Viehrig, In: C. Boller (Ed.), 6th European Workshop on Structural Health Monitoring, Dresden, Germany, vol. 1, 2012, pp. 138–145.
[32] C. Zurbuchen, H.W. Viehrig, F.P. Weiss, Nucl. Eng. Des. 239 (2009) 1246–1253.
[33] A. Ulbricht, J. Bohmert, H.-W. Viehrig, J. ASTM Int. 2 (2005) 151–164.
[34] G.R. Odette, T. Yamamoto, D. Klingensmith, Philos. Mag. 85 (2005) 779–797.
[35] R.E. Stoller, in: M.L. Grossbeck, T.R. Allen, R.G. Lott, A.S. Kumar (Eds.), Effects of Radiation on Materials: 21st International Symposium, ASTM STP 1447, ASTM International, West Conshohocken, PA, 2004, pp. 326–337.
[36] G.R. Odette, B.D. Wirth, J. Nucl. Mater. 251 (1997) 157–171.
[37] M.A. Sokolov, S. Spooner, G.R. Odette, B.D. Wirth, G.E. Lucas, in: R.K. Nanstad, M.L. Hamilton, F.A. Garner, A.S. Kumar (Eds.), Effects of Radiation on Materials: 18th International Symposium, ASTM STP 1325, American Society for Testing and Materials, West Conshohocken, PA, 1999, pp. 333–345.